

UC San Diego

UC San Diego Previously Published Works

Title

Globally ubiquitous negative effects of nitrogen dioxide on crop growth

Permalink

<https://escholarship.org/uc/item/5fg8r86r>

Journal

Science Advances, 8(22)

ISSN

2375-2548

Authors

Lobell, David B

Di Tommaso, Stefania

Burney, Jennifer A

Publication Date

2022-06-03

DOI

10.1126/sciadv.abm9909

Copyright Information

This work is made available under the terms of a Creative Commons Attribution-NonCommercial License, available at <https://creativecommons.org/licenses/by-nc/4.0/>

Peer reviewed

ENVIRONMENTAL STUDIES

Globally ubiquitous negative effects of nitrogen dioxide on crop growth

David B. Lobell^{1*}, Stefania Di Tommaso¹, Jennifer A. Burney²

Nitrogen oxides (NO_x) are among the most widely emitted pollutants in the world, yet their impacts on agriculture remain poorly known. NO_x can directly damage crop cells and indirectly affect growth by promoting ozone (O₃) and aerosol formation. We use satellite measures of both crop greenness and NO_x during 2018–2020 to evaluate crop impacts for five major agricultural regions. We find consistent negative associations between NO₂ and greenness across regions and seasons. These effects are strongest in conditions where O₃ formation is NO_x limited but remain significant even in locations where this pathway is muted, suggesting a role for direct NO_x damage. Using simple counterfactuals and leveraging published relationships between greenness and growth, we estimate that reducing NO_x levels to the current fifth percentile in each region would raise yields by ~25% for winter crops in China, ~15% for summer crops in China, and up to 10% in other regions.

INTRODUCTION

Improvements in agricultural productivity are needed in the coming decades to achieve many sustainable development goals, including reduced hunger and increased protection of forest area and biodiversity. Among the many strategies to achieve these gains are efforts to improve air quality (1). Although these efforts are primarily motivated by human health benefits, the potential agricultural effects are substantial. In some cases, levels of pollutants such as ozone are thought to suppress yields by as much as 30 to 40%, yet these estimates include wide uncertainties (2, 3). A better understanding of the agricultural impacts of air pollution would help to better assess both the potential benefits of air quality improvements and how prominent a role pollution reduction should have among efforts to raise agricultural productivity.

Historically, studies of air quality and crop productivity have been limited to small-scale experimental manipulations or observational analyses that rely on sparse ground measures of pollution. While these studies have provided a clear basis for further study, they are often plagued by large uncertainties associated with the difficulty of extrapolating beyond the experimental conditions (in the case of experiments) or the challenge of limited overlap between air monitoring stations and agricultural areas (in the case of empirical studies). These latter studies have also tended to focus on the secondary pollutants (ozone and particulate matter) that are most widely monitored because of human health concerns and have been limited to regions with available ground measures (4).

An alternative to using ambient measures of pollution has been to exploit yield variations in the vicinity of known pollution sources, such as power plants, including inspection of changes before and after the power plants are active (4–6). These approaches circumvent some of the drawbacks of relying on pollution monitoring stations, as they do not rely on direct pollution measures, can integrate the net effect of multiple pollutants, and can more readily assess the potential effect of removing specific pollution sources. However, approaches that rely on gradients near pollution sources can suffer

from an inability to distinguish effects of different pollutants, are limited to regions that have reliable inventories of, e.g., power plant activity, and can be confounded if other sources (e.g., transportation) contribute significantly to local pollution levels.

Fortunately, recent progress in satellite observations is leading to rapid advances in global air pollution monitoring. The Tropospheric Monitoring Instrument (TROPOMI) instrument, which was launched aboard the Sentinel-5 Precursor in late 2017, is especially novel in its ability to monitor tropospheric nitrogen dioxide (NO₂) levels at daily frequency, with monthly aggregations of these measures available at spatial resolutions as fine as 0.01° (~1 km at the equator) (7). NO₂ is itself a good measure of overall NO_x [NO_x, nitrogen oxide (NO) plus NO₂] (8).

Plant health is affected by NO_x via both direct and indirect pathways, some of which are illustrated in Fig. 1. NO and NO₂ are themselves phytotoxins that can directly damage plant growth and reduce yields (9). In addition, NO_x can operate through at least two indirect pathways. First, it is a key precursor to formation of ozone (O₃) in the troposphere, another phytotoxin known to reduce crop yields (10). Especially in seasons and regions with high levels of volatile organic compounds (VOCs), variations in NO₂ are tightly associated with variations in O₃ levels (11, 12). Second, NO_x is a precursor to particulate matter aerosols. In the presence of ammonia (often the case in agricultural regions from application of nitrogenous fertilizers such as urea), NO_x can result in increased concentrations of ammonium nitrate aerosols (NH₄NO₃) (13) and can also oxidize sulfur dioxide (SO₂) and drive formation of ammonium sulfate aerosols [(NH₄)₂SO₄] (14, 15). These particles reflect and scatter incoming sunlight, changing the radiation environment experienced by crops and reducing access to photosynthetically active radiation (16, 17). Other pathways not depicted in Fig. 1 include additional interactions among NO₂, nitrates, O₃, and SO₂ (18); the effects of NO_x on secondary aerosol formation; and effects of NO_x on the deposition of atmospheric nitrogen in agricultural fields.

Despite general understanding of NO_x's potential deleterious effects, few studies have attempted to quantify its impact on crops at scale. Several studies have examined measures of plant health or crop yield along gradients of pollution near urban areas (19, 20) or in fumigation experiments (21–24). In many of these cases, NO_x was just one of several pollutants, and only the combined effects of

Copyright © 2022
The Authors, some
rights reserved;
exclusive licensee
American Association
for the Advancement
of Science. No claim to
original U.S. Government
Works. Distributed
under a Creative
Commons Attribution
NonCommercial
License 4.0 (CC BY-NC).

¹Department of Earth System Science and Center on Food Security and the Environment, Stanford University, Stanford, CA, USA. ²School of Global Policy and Strategy, University of California San Diego, La Jolla, CA, USA.

*Corresponding author. Email: dlobell@stanford.edu

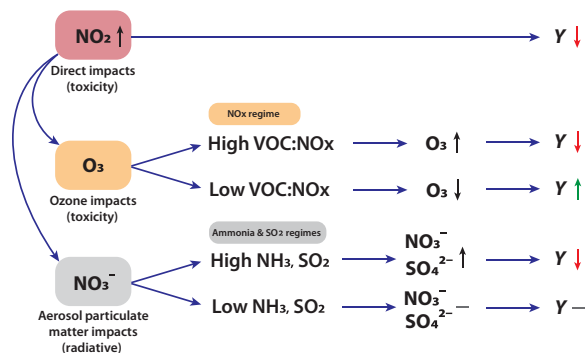


Fig. 1. Pathways of impact for NO₂ (NO_x) on crop yields. NO_x is itself a phytotoxin, and increased levels lead to decreased plant growth and lower yields. NO_x can also lead to formation of ozone, which is also toxic for crops, but the ozone dynamics depend on the local pollution regime. In areas that are NO_x limited but have high available reactive VOCs, increased NO_x leads to more ozone formation and decreased yields. In areas that are NO_x saturated (i.e., have low VOC:NO_x ratios), increased NO_x levels titrate ozone out of the atmosphere, lowering levels and resulting in increased yields. Last, increased NO_x in the presence of ammonia or SO₂ can lead to aerosol formation. These aerosols reflect and scatter incoming sunlight, reducing the amount of light available for photosynthesis and lowering yields. The net impact of NO₂ (NO_x) on crop yields, i.e., the sum of direct, ozone, and aerosol pathways, thus depends on the local pollution regime. We leverage different ozone regimes around the world to evaluate the relative importance of ozone pathway.

pollutants could be assessed. In other cases, experiments attempted to isolate the effect of NO_x, although typically on natural vegetation, not crops (21, 24). In general, these studies point to direct negative yield effects of NO_x exposure at values that are commonly found in agricultural regions. For example, the World Health Organization guidelines state a “no effect” level for vegetation of 15 to 20 μg/m³ for annual average NO₂ [roughly 8 to 11 parts per billion (ppb)] (25), whereas reported NO₂ levels in most regions commonly exceed these values (4, 7, 19). While previous studies thus indicate some role for direct NO_x effects, they report substantial variability across different plant species, treatments, levels of other pollutants, and temperature and radiation conditions and are therefore of limited utility in assessing overall yield impacts in farmers’ fields. To date, the lack of concurrent measures of NO_x exposure and crop yield has precluded progress on this issue.

In the current study, we combine the recent TROPOMI measures of NO₂ for 2018–2020 with satellite measures of crop greenness to elucidate the role of NO₂ in crop productivity. One benefit of focusing on NO₂ is that it is measured with more precision than most pollutants because of its unique spectral signature (8). Another substantial benefit is that NO₂ is a primary pollutant (i.e., directly emitted from pollution sources) rather than a secondary pollutant formed in the atmosphere (e.g., O₃ and NH₄NO₃), which makes it more straightforward to translate estimated impacts, even if they occur through multiple pathways, to the underlying emissions and possible control measures. This approach is less convoluted, for example, than calculating yield gains associated with a reduction in O₃ and then separately estimating the necessary NO_x reductions needed to achieve the O₃ reductions.

The use of satellite measures of greenness enables us to examine crop conditions at a resolution commensurate with the NO₂ measures, which would not be possible using administrative records of crop yields. Our preferred greenness measure, near-infrared reflectance of

vegetation (NIRv) (see Materials and Methods), has been shown in many recent studies to be linearly and strongly correlated with crop growth and yield (26–28). Satellite data thus offer a practical and robust way to measure both pollution exposure and crop growth, enabling us to examine the effects of NO₂ in multiple regions and years.

Here, we address three fundamental questions related to NO_x impacts for five major growing regions around the world. First, is there a clear negative association between NO₂ and crop productivity throughout different regions, consistent with the idea that NO_x is an important factor in crop growth? Second, how much does the effect of NO₂ differ by season and region, and what do these differences indicate about the direct versus indirect effects of NO_x? Third, what is the potential gain in crop productivity that could reasonably be expected if NO_x levels were reduced in each region?

RESULTS

We observed a wide range of crop exposure to NO₂ across major growing regions and seasons (Fig. 2). NO₂ levels were generally highest in the winter season, which leads to exposure of wheat and other winter crops to higher NO₂ levels than summer crops. Exposure was generally highest for crop locations in China, although not all areas in China experienced high levels. After China, exposure was highest in India and Western Europe, with both having many locations with exposures in terms of tropospheric vertical column density (TVCD) above 25 μmol m⁻². North and South America generally had the lowest exposures. All five regions exhibited a considerable range of exposures, even when examining variation within 1° × 1° or 0.5° × 0.5° areas within each region (fig. S1).

These local gradients of NO₂ (i.e., within roughly 50 km × 50 km) form the basis of our estimates of the impacts of NO₂, which rely on the degree to which the local de-meaned NO₂ variations are correlated with spatial variations in de-meaned peak greenness, as measured by the NIRv vegetation index (VI) (Fig. 3). This identification strategy relies only on local (~50 km) variation to estimate impacts because, while larger-scale spatial variations in both pollution and crop yields (e.g., northern versus southern China) can provide meaningful information, they also greatly increase the risk of confounding from omitted variables (29). We find that, in all five regions, there is a highly significant negative association between the two (Fig. 4).

Robustness checks indicate that these relationships are unlikely to arise because of artifacts in the NO₂ retrieval algorithms, specifically the reliance on surface albedo, which is itself influenced by vegetation (table S1). Similarly, results are unlikely to result from the spatial correlation of NO₂ with overall aerosols (of which nitrate aerosols are typically a small fraction) (30), given that results are robust to including controls for aerosol optical depth (fig. S2). Results are also robust to removing grid cells with a large fraction of non-cropland, which could potentially affect both NO₂ and greenness measures (fig. S3), using alternate sources of crop masks (fig. S4) and using alternate measures of crop greenness (fig. S4). These tests and the fact that estimated NO₂ effects were consistently negative across all study years (fig. S4) indicate that these estimates are very likely to reflect a true causal relationship between NO₂ and crop growth. However, these estimates alone cannot indicate the likely mechanism of impact.

To further distinguish between plausible pathways of impact, we partitioned each region into two subsets of observations. In the first subset, we identified points with a ratio of HCHO:NO₂ above 2,

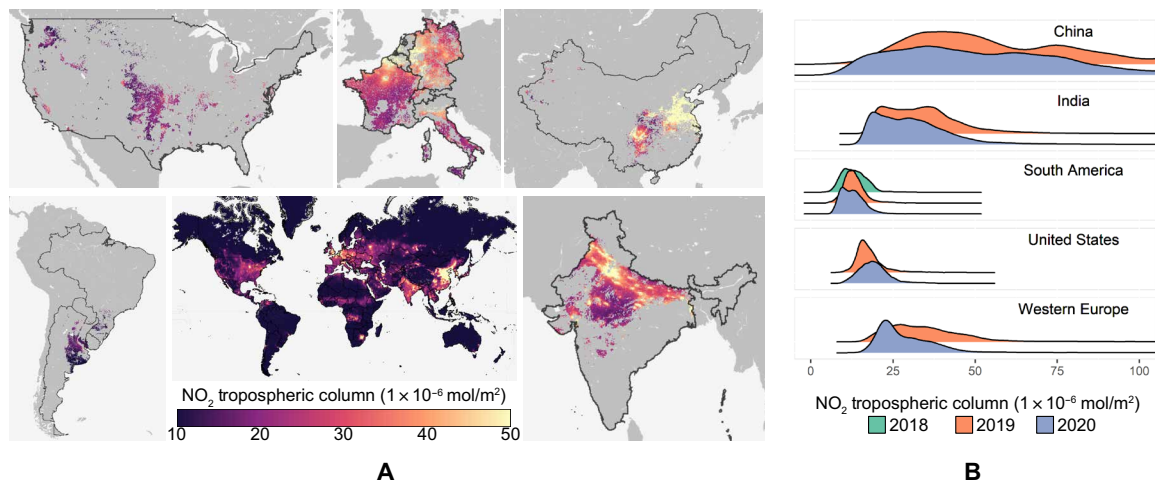


Fig. 2. Regional crop exposures to NO₂. (A) A map of average TROPOMI NO₂ values for the peak of the winter crop season for the world (April and May) and for the winter season for five regions of interest in this study. Regional insets only show pixels where wheat is more than 2% of the land area from which we sample data for our analysis. (B) Histograms of NO₂ values for the winter season for each region and year. The months associated with each region are given in table S2. A comparable figure for the summer season is shown in the Supplementary Materials (fig. S7).

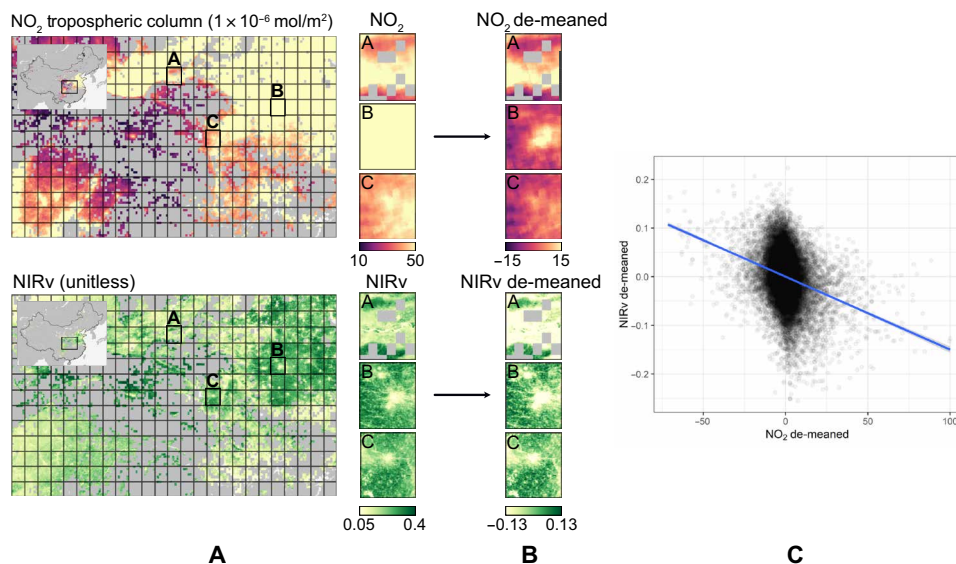


Fig. 3. Illustration of the fixed-effect regression approach. In each region and season, points are sampled throughout the region and split into local $0.5^\circ \times 0.5^\circ$ grid cells (A) (which shows NO₂ and NIRv values for 2020 in winter in China as an example). The deviations of NO₂ and NIRv values for each point from their grid cell average are then calculated (B), and the deviations for all grid cells are then combined into a single regression (C). Blue line in (C) shows best-fit linear regression line fit to all points. By taking deviations from the local averages, we reduce the chance that a third variable is correlated spatially with both NO₂ and NIRv, which could potentially lead to omitted variable bias.

which represents situations where O₃ formation is generally NO_x limited (11) and, therefore, where an increase in NO_x would be expected to lead to an increase in O₃. The second subset included all points with a ratio below 2, where O₃ is expected to be less responsive to variations in NO_x. For our study regions and seasons, only the winter season in China and Western Europe had a considerable fraction of points in both regimes, whereas in other cases, the cropped areas typically experience only the NO_x limited regime, with a ratio above 2 (Fig. 5, A and B).

When examining the NO₂ sensitivity separately by O₃ regime, we found that (i) NO₂ sensitivity was considerably higher for locations

where O₃ formation was likely to be NO_x limited and (ii) NO₂ sensitivity was still significantly negative in regimes where O₃ formation was not NO_x limited (Fig. 5, C and D). In both China and Europe, the sensitivity for NO_x-limited conditions was roughly double that for nonlimited conditions. These results suggest that O₃ is an important pathway for the impact of NO₂ but that other mechanisms including direct damage from NO₂ likely play an important role in suppressing crop growth, contributing perhaps as much as half of the total damage in some regions.

Table 1 presents an estimate of the total change in crop greenness (NIRv) that would be expected if all locations within a region

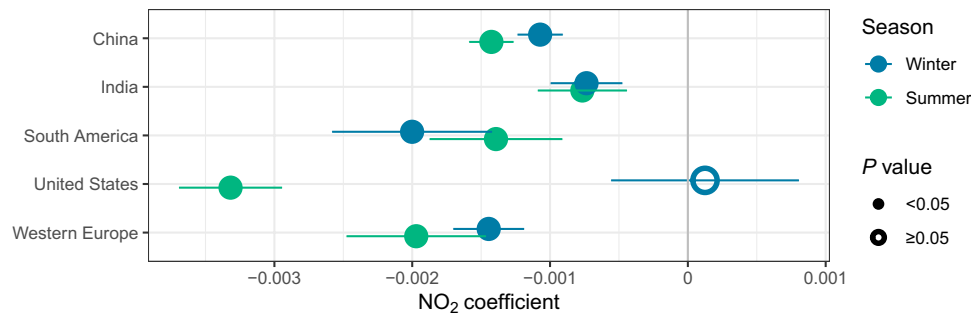


Fig. 4. Higher NO₂ is consistently associated with lower crop greenness. Points indicate the estimated effect of a 1-U increase of NO₂ on the NIRv, a measure of crop growth. Error bars show the 95% confidence interval based on SEs clustered at 0.5° × 0.5° grid cells. Solid colors denote estimates significant at $P < 0.05$. The figure shows the results of 10 separate regressions, one for each region and season, with multiple years pooled together. Figure S4 shows results of regressions run for individual years.

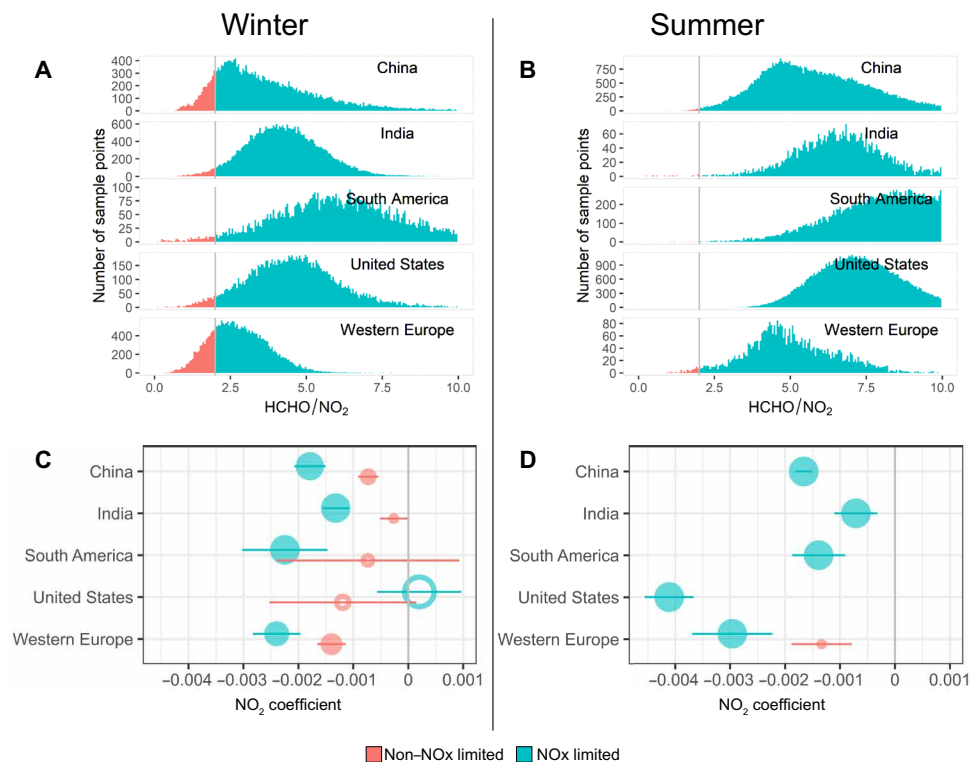


Fig. 5. NO₂ impacts are higher in NO_x-limited ozone regimes but persist even in non-NO_x limited regimes. (A and B) The distribution of the ratio of HCHO:NO₂ from TROPOMI for 2020 winter and summer cropping seasons in each region. Values above 2 are used to indicate NO_x-limited regimes. (C and D) Estimated sensitivity of greenness to NO₂ for two different subsets of points, with points split by the ozone regime. The point sizes are proportional to the percentage of points by regime type in each region. Error bars indicate the 95% confidence intervals.

were to achieve NO₂ levels equal to the fifth percentile of observed levels over the study period. This represents a simplistic scenario of aggressive actions to curb NO₂ and is not meant to substitute for a more detailed analysis of specific control measures but rather to bracket the total possible gain from reducing NO₂. A more extreme scenario, whereby all locations are reduced to zero, was not considered since this would extrapolate beyond the support of the data used to estimate the regressions.

Table 1 and Fig. 6 also estimate the total yield gain that would be associated with this increase in NIRv. To translate NIRv to yield gain, we rely on the fact that crop photosynthetic activity has been shown to be linearly related to NIRv (26) (see Materials and Methods). We

estimate that reduction of NO₂ could contribute significantly toward yield gains in many cases, with the largest gains estimated for China: 28% in winter and 16% in summer. Western Europe would also experience substantial gains of nearly 10% for both winter and summer crops, with gains in India of roughly 8% in summer and 6% in winter.

DISCUSSION

The effects of NO₂ estimated in this study represent the net impact of myriad complex processes that govern both atmospheric chemistry (e.g., the conversion of NO₂ to other pollutants) and plant biology (e.g., the ability of plants to recover from exposure to high levels of

Table 1. Summary of coefficients for NIRv regression, average and fifth percentile of NO₂ levels, and gains for reductions to fifth percentile for each region and season. Values in parentheses indicate 1 SE. Units of βNO_2 are NIRv change per micromole/meter² NO₂, and units of NO₂ are micromole/meter². Values shown in table assume NIRv₀ equal to 0.07.

Winter season

Region	βNO_2	NO ₂ average	NO ₂ fifth percentile	NO ₂ difference	NIRv gain	Yield gain (%)
China	-0.0011 (0.0001)	57	18	39	0.042	27.9 (2.2)
India	-0.0007 (0.0001)	33	18	15	0.011	6.4 (1.2)
South America	-0.0020 (0.0003)	13	8	5	0.010	7.4 (1.1)
United States	0.0001 (0.0003)	18	13	6	-0.001	-0.6(1.8)
W Europe	-0.0014 (0.0001)	33	19	13	0.019	8.7 (0.8)
Summer season						
China	-0.0014 (0.0001)	35	15	20	0.029	17.1 (1)
India	-0.0008 (0.0002)	26	15	11	0.008	5.3 (1.1)
South America	-0.0014 (0.0002)	11	7	4	0.005	2.1 (0.4)
United States	-0.0033 (0.0002)	22	16	7	0.022	8.7 (0.5)
W Europe	-0.0020 (0.0003)	31	20	10	0.020	10.6 (1.4)

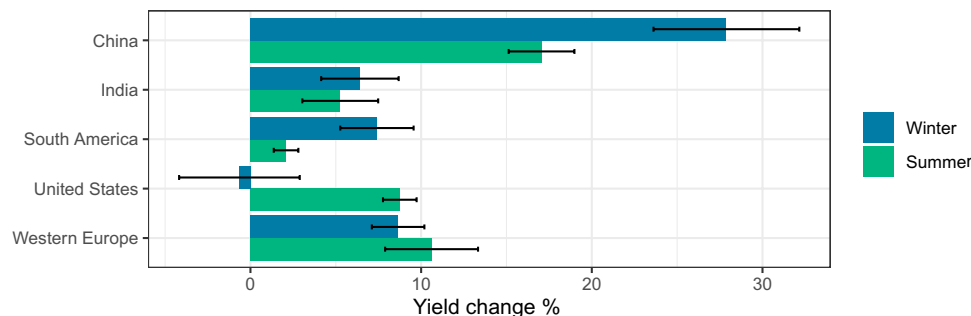


Fig. 6. Reductions in NO₂ would lead to substantial yield gains in many regions. Bars show estimate of mean yield increase in each region and season associated with a hypothetical reduction of NO₂ levels to the fifth percentile observed for the respective region and season. Error bars indicate the 95% confidence intervals, which reflect the uncertainties in crop responses shown in Fig. 4.

NO₂ or O₃). This integration over many processes is both a strength and weakness of our study. By directly relating NO₂ to crop productivity, we capture the net effects of many pathways of impact and recovery in actual farmers' fields, which encompass a diversity of conditions that would be impossible to recreate in controlled experiments. At the same time, the inability to fully disentangle mechanisms can limit the understanding of how effective different potential interventions would be at lowering impacts and can complicate comparisons with prior studies.

For example, comparison with the many prior studies that have considered the effects of O₃ on crop growth are difficult because (i) we are capturing effects of multiple pathways by which NO_x can affect yields, with O₃ being just one of these pathways, (ii) we likely fail to fully capture O₃ effects because the longer residence time of O₃ means that O₃ concentrations are imperfectly correlated with NO₂, and (iii) other studies may inadvertently capture some (but not all) NO_x effects in their estimates of O₃ damages since NO_x is correlated with O₃ and empirical studies that do not measure NO_x will misattribute some direct NO_x effects to O₃.

Despite these caveats, comparison of our results with prior O₃ studies reveals several similarities. First, we find that the biggest

estimated impacts among all locations and seasons are for winter crops in China. This result is similar to Mills *et al.* (31), who identified China as having the largest estimated wheat yield loss out of all wheat-producing countries on the basis of an analysis of exposure to O₃ above 40 ppb.

Second, similar to studies with O₃ (1, 2), our results indicate that reducing pollution would result in substantial yield gains. Here, we considered reducing NO₂ levels to the fifth percentile observed in the region. This scenario may be more conservative than studies that consider theoretically reducing O₃ exposure to zero, although, since O₃ exposure is often measured above some threshold (e.g., 60 ppb), reducing NO₂ by 50% could lead to far greater than 50% reduction in these O₃ metrics. In addition, reducing NO₂ levels to zero is unrealistic, given that lightning contributes a small but nontrivial fraction of global tropospheric NO_x (32).

In China, we estimate a 28% yield gain for winter crops from reducing NO₂ to background levels (i.e., fifth percentile). For wheat, the main winter crop, an empirical study (33) estimated that each 10% reduction in O₃ would lead to a 2.5% increase in wheat yields, implying a total of 25% gain from removing O₃. Studies that use dose-response functions from experimental studies and then apply

these to observed O_3 levels result in fairly wide ranges, given the uncertainty in both O_3 exposures and response functions. For example, Mills *et al.* (31) estimated between 12 and 25% yield loss for wheat in China depending on the ozone metric used. A recent analysis focused on China estimated potential gains from eliminating O_3 of 21 to 39% for winter wheat, 3.9 to 14% for rice, and 2.2 to 5.5% for maize (34). Thus, our estimate of ~28% gains possible from reduced air pollution is consistent with prior work focused on O_3 . In addition, similar to other studies, we find that gains for summer crops would be roughly half as large as for winter, given that NO_2 levels are generally lower in summer.

In India, we estimate gains from NO_2 reductions that are ~6 to 8% for both winter and summer seasons (Fig. 6). A recent review of O_3 studies for India wheat estimates 21% yield gains for elimination of O_3 (35), roughly double our estimate for NO_2 . One source of this disparity is likely the fact that the fifth percentile of NO_2 in India is roughly half the mean value, so our reduction scenario would likely leave a considerable amount of O_3 exposure.

In general, our estimated sensitivities to NO_2 are higher for summer than winter seasons (Fig. 4). Although there are many differences between the two seasons that could plausibly explain this pattern, it is likely that the indirect effects via O_3 are stronger in the summer, both because overall O_3 concentrations are typically higher in summer and the O_3 regime is more NO_x limited in the summer (Fig. 5). Similarly, the indirect pathway via NH_4NO_3 - or NO_2 -driven formation of sulfate aerosols is plausibly higher when more NH_3 is present, although this relationship is complicated by meteorological factors and the presence of other aerosol precursors in the environment (e.g., SO_2) and likely varies by region. We thus do not attempt to isolate the role of the aerosol pathway, which would require assumptions about the proportion of NH_4NO_3 to overall aerosols and the direct effect of each aerosol type on the greenness measures. However, the fact that NH_3 levels are generally higher in summer (fig. S5) is consistent with enhanced aerosol formation in general. Temperature and radiation regimes also likely play some role, although previous work suggested that damage from NO_2 was smaller, not larger, under high radiation regimes (21).

Overall, we find a remarkably consistent negative association between NO_2 and crop growth in major cropping regions. The persistence of these negative effects across many conditions, including when NO_x is not limiting O_3 formation, indicates a significant role for direct phytotoxicity of NO_2 . At the same time, effects appear most negative in seasons and locations where NO_x likely drives O_3 formation, indicating that indirect pathways are also important. These results indicate that reduction of NO_x emissions could have important benefits for crop production, sometimes exceeding 30% of current yields. The magnitude of these effects have the potential both to alter overall yield growth rates (which are typically ~1% per year) and substantially change cost-benefit analysis for pollution mitigation measures (36, 37).

Maps of the spatial pattern of impacts (fig. S6) indicate that yield gradients from ambient NO_2 can be substantial within a region, with impacts differing by up to 50%. At first glance, the strong negative yield impacts in China and India may appear at odds with recent reports of substantial greening of vegetation in these countries, with much of that greening associated with croplands (38). However, trends in greenness should respond to trends in NO_2 rather than average levels, and the trends in greenness in China are highest in the same areas (around the North China plain) that have experienced

significant declines in NO_2 since 2005 (39). Similarly, greenness trends in India were strongest in the northwest, which has experienced much smaller increases in NO_2 than the rest of the country (39). Thus, while detailed trend analysis is not possible with the short TROPOMI record, the estimated importance of NO_2 reported here is consistent with prior independent analyses of global greenness trends and NO_2 trends.

We anticipate several fruitful directions for future work. Incorporation of other spaceborne measures of crop activity, including measures of photosynthetic activity from solar-induced fluorescence (SIF) (40, 41), could help to probe the mechanisms of NO_2 effects and the differential sensitivity of crops throughout the growing season. More detailed examination of other pollutants, such as SO_2 and NH_3 , and meteorological variables could help to understand variation in NO_2 sensitivity across different regions, years, and seasons. Notwithstanding these remaining research gaps, the consistent negative impact of NO_2 crops across diverse conditions reported here is an important advancement in our understanding of the widespread role that air pollution plays in crop production.

MATERIALS AND METHODS

Study regions

To link NO_2 measures to crop performance, we first define five regions of interest corresponding to major agricultural areas: the United States, China, India, Western Europe, and South America (Fig. 2). In each region, we separately analyze winter and summer crop behaviors.

MODIS greenness

To measure crop performance, we rely on two VIs calculated based on MODIS (Moderate Resolution Imaging Spectroradiometer) Terra MOD09A1 version 6 product (<https://lpdaac.usgs.gov/products/mod09a1v006/>), which represents 8-day composites of surface spectral reflectance at a 500-m resolution. The first is the common normalized difference VI (NDVI) (42), which is a conventional measure of plant greenness but often suffers from saturation for denser canopies. As a second measure, we use the NIRv, which is the product of NDVI and NIR reflectance (43). The NIRv has shown strong linear correlations with crop productivity at seasonal scales (26, 27), as well as final yields (28), and is therefore used as our primary measure of crop growth. All greenness measures were resampled to 1 km to match the TROPOMI resolution. Using VI time series for each region and crop, we identify the 2 months corresponding to the peak of the season for that crop (table S2). We opt for greenness measures rather than SIF measures that arguably more directly capture spatial and temporal variations in vegetation growth (44–46). This decision was based primarily on the availability of gridded data products and the relatively coarse spatial resolution of current SIF products compared to MODIS. We leave exploration of SIF to future work, which could particularly be useful for examining effects of subseasonal variations in pollution exposure.

TROPOMI NO_2 and HCHO

We use NO_2 measures from the TROPOMI aboard the Copernicus Sentinel-5 Precursor satellite. Specifically, we use the OFFL L3 (offline level 3)–processed data available in Google's Earth Engine platform (47), which provides daily estimates at $0.01^\circ \times 0.01^\circ$ (~1 km) resolution since late June of 2018. Following existing recommendations (8), only points

with a quality assurance (QA) value above 75% were used for analysis. Although the TROPOMI instrument is sensitive to the total column NO₂, the baseline processing method uses model simulations to partition NO₂ into stratospheric and tropospheric column densities. We use the TVCD band as a proxy for variation in surface NO₂ concentrations.

The algorithm for separation of stratospheric and tropospheric NO₂ subtracts stratospheric-modeled NO₂ from the total observed column. This separation is feasible, both because there is not much exchange of NO₂ from the troposphere to the stratosphere (except for volcanoes) (48) and the variations in stratospheric NO₂ are driven by solar insolation at diurnal, annual, and multiannual scales (49), whereas lower tropospheric levels are driven by anthropogenic emissions. Although stratospheric concentrations can be of the same order as near-surface levels, their distinctive patterns and profiles facilitate the partitioning at the tropopause. Moreover, variations within the troposphere are mainly driven by surface variations, because surface concentrations are typically two orders of magnitude larger than in the upper troposphere (50, 51). For these reasons, the TVCD derived from the TROPOMI algorithm has shown strong agreement with surface station measurements, for instance, with TROPOMI capturing two-thirds of the variation in 2019 annual averages across sites in the United States (30). Regridding of TROPOMI from its native resolution to a 1-km resolution has also been shown to improve agreement with surface measurements (7), motivating our choice of using the 0.01° × 0.01° data in the current study.

For analysis of different O₃ regimes, we also use TROPOMI measures of HCHO column densities available in Earth Engine. These data are available starting in December 2018 and have the same spatial and temporal resolution as the NO₂ data. We calculate the ratio of HCHO to NO₂ as an indicator of the O₃ regime, following Duncan *et al.* (11). Specifically, we first take bimonthly (2-month) averages of NO₂ and HCHO and then calculate the ratio of HCHO:NO₂ using the bimonthly averages. Negative daily values are included in the calculation of the averages, but the small number (129) of bimonthly averages that are negative are removed from further analysis.

Weather

To control for weather variation, which can influence both NO₂ and greenness, we use TerraClimate monthly data (52) to retrieve early and late season precipitation and vapor pressure deficits.

Crop area

To ensure that the MODIS and TROPOMI measures used in this study correspond to agricultural locations, we require a globally complete map of areas for specific crops. For this, we use the Spatial Production Allocation Model 2005 (53), which has 10 km × 10 km spatial resolution, and create crop-specific masks, considering only cells with at least 2% of the area sown to the crop. For winter crop, we use the wheat mask, whereas for summer crops, we use the maize mask as our primary filter. Maize is a common summer crop in all regions, although it is typically sown in a landscape that includes many other crops, such as soybean, rice, or canola. Thus, maize is used as a proxy for the location and timing of summer crops. Because rice is also prevalent in India and China in many locations without maize, we repeated the analysis for these two regions using rice for comparison with the results for maize. In addition, we also vary the threshold on crop area from 2% to much higher values because of concerns that variation in land cover within grid cells could drive some of our results but find that this is not the case (fig. S3).

Sampling points

Using crop-specific crop masks, we sample a large number of cells within each region, with a density of sampling meant to ensure similar densities across the regions (table S2) and extract bimonthly NO₂, VIs, and weather values for these cells for July 2018 to April 2020.

We then remove cells for which the crop is likely not a major contributor to pixel greenness, retaining only cells for which the peak of the monthly NDVI values occurs in one of the 2-month window defined using MODIS time series (table S2).

Other dataset used for robustness checks

Some additional datasets were not used in the main specifications but for performing robustness checks or additional analysis. To examine possible influence of albedo on the NO₂ retrieval algorithm, we used the OMI (Ozone Monitoring Instrument)/Aura Surface Reflectance Climatology L3 product, OMILER (OMI Lambert equivalent reflectivity) at 440 nm at a spatial resolution of 0.5° by 0.5° (downloaded at https://disc.gsfc.nasa.gov/datasets/OMILER_003/summary). To examine the potential pathway related to NH₄NO₃ aerosols or sulfate aerosol formation driven by NO₂, we used the standard monthly L3 product (total column) for NH₃ from IASI (infrared atmospheric sounding interferometer)/Metop-A at 1° × 1° (downloaded at <https://iasi.aeris-data.fr/NH3/>). To examine the potential for confounding from overall aerosol levels, we used MODIS Terra and Aqua combined Multi-angle Implementation of Atmospheric Correction Land Aerosol Optical Depth (MCD19A2 V6) based on gridded level 2 product produced daily at a 1-km resolution (<https://lpdaac.usgs.gov/products/mcd19a2v006/>).

Regression model

To estimate the effect of NO₂ on greenness, we statistically relate collocated NO₂ levels and VIs and estimate best-fit parameters for the following model separately for each region and season

$$VI_{i,t} = \beta NO_2 * NO_{2,i,t} + \beta_w * W_{i,t} + a_{LL,i} + c_t + e_{i,t} \quad (1)$$

Here $VI_{i,t}$ refers to the observed peak VI for location i in year t , $NO_{2,i,t}$ is the observed average value of TVCD of NO₂ during the peak months of the growing season, $W_{i,t}$ is a vector of weather controls for the growing season, $a_{LL,i}$ represents a local intercept (fixed effect) for the area surrounding location i (e.g., for each 0.5° latitude × 0.5° longitude cell), c_t is a year fixed effect, and $e_{i,t}$ represents the residual noise. The fixed effects for both the local area and the year are intended to control for the unobserved factors that might affect VI and be correlated with NO₂, so that Eq. 1 relies on local spatial gradients (i.e., de-measured values) for identification of βNO_2 . Since weather is of particular concern, both because rainfall could stimulate crop growth and clean pollution from the air and because temperature could affect crop growth and ozone formation, we also include specific controls for weather, namely the total precipitation and average vapor pressure deficit during the same months as NO₂. Removal of the weather controls has negligible effects on the results. SEs for coefficients were calculated using clustering at the 0.5° grid cell level.

Other potential sources of concern are that aerosol is correlated with NO₂ and yet artificially lowers the estimated greenness or gradients in land use within grid cells lead to changes in both NO₂ and greenness without a causal relationship between the two. We therefore test the sensitivity of results to inclusion of aerosol measures and to restricting our sample to grid cells with high percentages of cropland, finding the results robust to either change (figs. S2 and S3).

We pool data across all years to calculate a single regression for each region and season, although we also perform regressions by year to confirm that results are consistent across time (fig. S4). To assess the role of direct versus indirect pathways, we also estimate Eq. 1 for subsets of observations in each region based on the NO_x regime, where the NO_x regime is defined as either NO_x limited if the ratio HCHO:NO₂ is above 2 or non-NO_x limited if the ratio is below 2 (see Fig. 4) (11).

Estimate of yield increases from NO₂ reductions

To estimate the increase in canopy greenness for a counterfactual scenario of low NO₂, we calculate for each region and season

$$\text{NO}_{2,\text{dif}} = \text{NO}_{2,\text{avg}} - \text{NO}_{2,5\text{th}} \quad (2)$$

Where NO_{2,avg} is the average level and NO_{2,5th} is the fifth percentile of observed values over the study period over all locations (i.e., grid cells) and years for that region and season. We use the fifth percentile as a simple scenario of aggressive actions to curb NO₂, which we consider as an upper bound on the near-term potential to reduce NO₂. A more extreme scenario, whereby all locations are reduced to zero, was not considered, since this would extrapolate beyond the support of the data used to estimate the regressions.

The estimated best-fit coefficient $\hat{\beta}\text{NO}_2$ in Eq. 1 represents the expected change in canopy greenness (i.e., NIRv or NDVI) for a unit change in NO₂ TVCD. To translate these results into estimates of yield change per unit of NO₂, we consider crop yield (*Y*) to linearly increase with NIRv

$$Y = \beta_{\text{NIRv}} * (\text{NIRv} - \text{NIRv}_0) \quad (3)$$

where NIRv₀ is the NIRv value for which the crop growth is zero. This functional form is supported by several studies showing a clear linear relationship between NIRv and crop gross primary photosynthesis (GPP) as well as studies that show crop GPP to be linearly associated with yield (40, 54). We set NIRv₀ equal to 0.07 based on Badgley *et al.* (26).

The yield in current conditions can then be expressed as

$$Y_{\text{cur}} = \beta_{\text{NIRv}} * (\text{NIRv}_{\text{cur}} - \text{NIRv}_0) \quad (4)$$

Where NIRv_{cur} is the current average of NIRv. The yield in a counterfactual low NO₂ scenario can similarly be expressed as

$$Y_{\text{low NO}_2} = \beta_{\text{NIRv}} * (\text{NIRv}_{\text{cur}} + \hat{\beta}\text{NO}_2 * \text{NO}_{2,\text{dif}} - \text{NIRv}_0) \quad (5)$$

The percent change in yield for the counterfactual low NO₂ scenario is then

$$\% \text{yield change} = \frac{Y_{\text{low NO}_2}}{Y_{\text{cur}}} - 1 = \frac{(\text{NIRv}_{\text{cur}} + \hat{\beta}\text{NO}_2 * \text{NO}_{2,\text{dif}} - \text{NIRv}_0) w}{(\text{NIRv}_{\text{cur}} - \text{NIRv}_0) w} - 1 \quad (6)$$

Substituting NIRv₀ equal to 0.06 or 0.08 into Eq. 6 resulted in small changes in the estimated yield impacts, typically less than 2%.

SUPPLEMENTARY MATERIALS

Supplementary material for this article is available at <https://science.org/doi/10.1126/sciadv.abm9909>

REFERENCES AND NOTES

1. D. Shindell, J. C. I. Kuylensstierna, E. Vignati, R. van Dingenen, M. Amann, Z. Klimont, S. C. Anenberg, N. Muller, G. Janssens-Maenhout, F. Raes, J. Schwartz, G. Faluvegi, L. Pozzoli, K. Kupiainen, L. Höglund-Isaksson, L. Emberson, D. Streets, V. Ramanathan, K. Hicks, N. T. K. Oanh, G. Milly, M. Williams, V. Demkine, D. Fowler, Simultaneously mitigating near-term climate change and improving human health and food security. *Science* **335**, 183–189 (2012).
2. S. Avnery, D. L. Mauzerall, J. Liu, L. W. Horowitz, Global crop yield reductions due to surface ozone exposure: 1. Year 2000 crop production losses and economic damage. *Atmos. Environ.* **45**, 2284–2296 (2011).
3. R. Van Dingenen, F. J. Dentener, F. Raes, M. C. Krol, L. Emberson, J. Cofala, The global impact of ozone on agricultural crop yields under current and future air quality legislation. *Atmos. Environ.* **43**, 604–618 (2009).
4. D. B. Lobell, J. A. Burney, Cleaner air has contributed one-fifth of US maize and soybean yield gains since 1999. *Environ. Res. Lett.* **16**, 074049 (2021).
5. K. Metaxoglou, A. Smith, Productivity spillovers from pollution reduction: Reducing coal use increases crop yields. *Am. J. Agric. Econ.* **0**, 259–280 (2019).
6. J. A. Burney, The downstream air pollution impacts of the transition from coal to natural gas in the United States. *Nat. Sustain.* **3**, 152–160 (2020).
7. A. Cersosimo, C. Serio, G. Masiello, TROPOMI NO₂ tropospheric column data: Regridding to 1 km grid-resolution and assessment of their consistency with in situ surface observations. *Remote Sens. (Basel)* **12**, 2212 (2020).
8. J. H. G. M. Van Geffen, H. J. Eskes, K. F. Boersma, J. P. Veeffkind, TROPOMI ATBD of the total and tropospheric NO₂ data products [Document number S5P-KNMI-L2-0005-RP, Issue 2.2.0; Royal Netherlands Meteorological Institute (KNMI), 2021]; <https://sentinel5.copernicus.eu/documents/247904/2476257/Sentinel-5P-TROPOMI-ATBD-NO2-data-products>.
9. World Health Organization, Effects of nitrogen containing air pollutants: Critical levels, in *Air Quality Guidelines Europe* (World Health Organization, ed. 2, 2000), pp. 288.
10. G. Mills, H. Pleijel, C. S. Malley, B. Sinha, O. R. Cooper, M. G. Schultz, H. S. Neufeld, D. Simpson, K. Sharps, Z. Feng, G. Gerosa, H. Harmens, K. Kobayashi, P. Saxena, E. Paoletti, V. Sinha, X. Xu, Tropospheric Ozone Assessment Report: Present-day tropospheric ozone distribution and trends relevant to vegetation. *Elem. Sci. Anth.* **6**, 47 (2018).
11. B. N. Duncan, Y. Yoshida, J. R. Olson, S. Sillman, R. V. Martin, L. Lamsal, Y. Hu, K. E. Pickering, C. Retscher, D. J. Allen, J. H. Crawford, Application of OMI observations to a space-based indicator of NO_x and VOC controls on surface ozone formation. *Atmos. Environ.* **44**, 2213–2223 (2010).
12. F. Zhao, C. Liu, Z. Cai, X. Liu, J. Bak, J. Kim, Q. Hu, C. Xia, C. Zhang, Y. Sun, W. Wang, J. Liu, Ozone profile retrievals from TROPOMI: Implication for the variation of tropospheric ozone during the outbreak of COVID-19 in China. *Sci. Total Environ.* **764**, 142886 (2021).
13. S. K. Kharol, R. V. Martin, S. Philip, S. Vogel, D. K. Henze, D. Chen, Y. Wang, Q. Zhang, C. L. Heald, Persistent sensitivity of Asian aerosol to emissions of nitrogen oxides. *Geophys. Res. Lett.* **40**, 1021–1026 (2013).
14. N. Unger, D. T. Shindell, D. M. Koch, D. G. Streets, Cross influences of ozone and sulfate precursor emissions changes on air quality and climate. *Proc. Natl. Acad. Sci. U.S.A.* **103**, 4377–4380 (2006).
15. J. Wang, J. Li, J. Ye, J. Zhao, Y. Wu, J. Hu, D. Liu, D. Nie, F. Shen, X. Huang, D. D. Huang, D. Ji, X. Sun, W. Xu, J. Guo, S. Song, Y. Qin, P. Liu, J. R. Turner, H. C. Lee, S. Hwang, H. Liao, S. T. Martin, Q. Zhang, M. Chen, Y. Sun, X. Ge, D. J. Jacob, Fast sulfate formation from oxidation of SO₂ by NO₂ and HONO observed in Beijing haze. *Nat. Commun.* **11**, 2844 (2020).
16. J. Proctor, Atmospheric opacity has a nonlinear effect on global crop yields. *Nat. Food*, **2**, 166–173 (2021).
17. J. Proctor, S. Hsiang, J. Burney, M. Burke, W. Schlenker, Estimating global agricultural effects of geoengineering using volcanic eruptions. *Nature* **560**, 480–483 (2018).
18. M. Gen, R. Zhang, D. D. Huang, Y. Li, C. K. Chan, Heterogeneous SO₂ oxidation in sulfate formation by photolysis of particulate nitrate. *Environ. Sci. Technol. Lett.* **6**, 86–91 (2019).
19. M. Agrawal, B. Singh, M. Rajput, F. Marshall, J. N. B. Bell, Effect of air pollution on peri-urban agriculture: A case study. *Environ. Pollut.* **126**, 323–329 (2003).
20. A. Singh, S. B. Agrawal, D. Rathore, Amelioration of Indian urban air pollution phytotoxicity in *Beta vulgaris* L. by modifying NPK nutrients. *Environ. Pollut.* **134**, 385–395 (2005).
21. T. A. Mansfield, P. H. Freer-Smith, Effects of urban air pollution on plant growth. *Biol. Rev. Camb. Philos. Soc.* **56**, 343–368 (1981).
22. S. Nussbaum, M. Geissmann, J. Fuhrer, Effects of nitric oxide and ozone on spring wheat (*Triticum aestivum*). *Water Air Soil Pollut.* **85**, 1449–1454 (1995).
23. P. I. Lane, J. N. B. Bell, The effects of simulated urban air pollution on grass yield: Part I—Description and simulation of ambient pollution. *Environ. Pollution. Ser. B Chem. Phys.* **8**, 245–263 (1984).
24. J. N. B. Bell, S. L. Honour, S. A. Power, Effects of vehicle exhaust emissions on urban wild plant species. *Environ. Pollut.* **159**, 1984–1990 (2011).
25. World Health Organization, Effects of nitrogen containing air pollutants: Critical levels, in *Air Quality Guidelines Europe* (World Health Organization, ed. 2, 2000).

26. G. Badgley, L. D. L. Anderegg, J. A. Berry, C. B. Field, Terrestrial gross primary production: Using NIRV to scale from site to globe. *Glob. Chang. Biol.* **25**, 3731–3740 (2019).
27. B. Dechant, Y. Ryu, G. Badgley, Y. Zeng, J. A. Berry, Y. Zhang, Y. Goulas, Z. Li, Q. Zhang, M. Kang, J. Li, I. Moya, Canopy structure explains the relationship between photosynthesis and sun-induced chlorophyll fluorescence in crops. *Remote Sens. Environ.* **241**, 111733 (2020).
28. L. Li, B. Wang, P. Feng, D. Li Liu, Q. He, Y. Zhang, Y. Wang, S. Li, X. Lu, C. Yue, Y. Li, J. He, H. Feng, G. Yang, Q. Yu, Developing machine learning models with multi-source environmental data to predict wheat yield in China. *Comput. Electron. Agric.* **194**, 106790 (2022).
29. H. Druckenmiller, S. Hsiang, “Accounting for unobservable heterogeneity in cross section using spatial first differences,” Working paper, National Bureau of Economic Research, 2018.
30. W. C. Malm, B. A. Schichtel, M. L. Pitchford, L. L. Ashbaugh, R. A. Eldred, Spatial and monthly trends in speciated fine particle concentration in the United States. *J. Geophys. Res. Atmos.* **109**, D03306 (2004).
31. G. Mills, K. Sharps, D. Simpson, H. Pleijel, M. Broberg, J. Uddling, F. Jaramillo, W. J. Davies, F. Dentener, M. Van den Berg, M. Agrawal, S. B. Agrawal, E. A. Ainsworth, P. Büker, L. Emberson, Z. Feng, H. Harmens, F. Hayes, K. Kobayashi, E. Paoletti, R. Van Dingenen, Ozone pollution will compromise efforts to increase global wheat production. *Glob. Chang. Biol.* **24**, 3560–3574 (2018).
32. L. T. Murray, Lightning NO_x and impacts on air quality. *Curr. Pollut. Reports* **2**, 115–133 (2016).
33. F. Yi, F. Jiang, F. Zhong, X. Zhou, A. Ding, The impacts of surface ozone pollution on winter wheat productivity in China—An econometric approach. *Environ. Pollut.* **208**, 326–335 (2016).
34. Y. Lin, F. Jiang, J. Zhao, G. Zhu, X. He, X. Ma, S. Li, C. E. Sabel, H. Wang, Impacts of O₃ on premature mortality and crop yield loss across China. *Atmos. Environ.* **194**, 41–47 (2018).
35. T. Fischer, Wheat yield losses in India due to ozone and aerosol pollution and their alleviation: A critical review. *Outlook Agric.* **48**, 181–189 (2019).
36. N. Scovronick, D. Anthoff, F. Dennig, F. Errickson, M. Ferranna, W. Peng, D. Spears, F. Wagner, M. Budolfson, The importance of health co-benefits under different climate policy cooperation frameworks. *Environ. Res. Lett.* **16**, 055027 (2021).
37. T. Vandyck, K. Keramidis, A. Kitous, J. V. Spadaro, R. Van Dingenen, M. Holland, B. Saveyn, Air quality co-benefits for human health and agriculture counterbalance costs to meet Paris Agreement pledges. *Nat. Commun.* **9**, 4939 (2018).
38. C. Chen, T. Park, X. Wang, S. Piao, B. Xu, R. K. Chaturvedi, R. Fuchs, V. Brovkin, P. Ciais, R. Fensholt, H. Tommervik, G. Bala, Z. Zhu, R. R. Nemani, R. B. Myneni, China and India lead in greening of the world through land-use management. *Nat. Sustain.* **2**, 122–129 (2019).
39. S. Jamali, D. Klingmyr, T. Tagesson, Global-scale patterns and trends in tropospheric NO₂ concentrations, 2005–2018. *Remote Sens.* **12**, 3526 (2020).
40. K. Guan, J. A. Berry, Y. Zhang, J. Joiner, L. Guanter, G. Badgley, D. B. Lobell, Improving the monitoring of crop productivity using spaceborne solar-induced fluorescence. *Glob. Chang. Biol.* **22**, 716–726 (2016).
41. L. Guanter, Y. Zhang, M. Jung, J. Joiner, M. Voigt, J. A. Berry, C. Frankenberg, A. R. Huete, P. Zarco-Tejada, J.-E. Lee, M. S. Moran, G. Ponce-Campos, C. Beer, G. Camps-Valls, N. Buchmann, D. Gianelle, K. Klumpp, A. Cescatti, J. M. Baker, T. J. Griffis, Global and time-resolved monitoring of crop photosynthesis with chlorophyll fluorescence. *Proc. Natl. Acad. Sci. U.S.A.* **111**, E1327–E1333 (2014).
42. J. W. Rouse, R. H. Haas, J. A. Schell, D. W. Deering, in *Proceedings of the Third ERTS Symposium* (NASA SP-351, 1973), vol. 1, pp. 309–317.
43. G. Badgley, C. B. Field, J. A. Berry, Canopy near-infrared reflectance and terrestrial photosynthesis. *Sci. Adv.* **3**, 1602244 (2017).
44. L. Guanter, C. Bacour, A. Schneider, I. Aben, T. A. Van Kempen, F. Maignan, C. Retscher, P. Köhler, C. Frankenberg, J. Joiner, Y. Zhang, The TROPISIF global sun-induced fluorescence dataset from the Sentinel-5P TROPOMI mission. *Earth Syst. Sci. Data.* **13**, 5423–5440 (2021).
45. T. S. Magney, D. R. Bowling, B. A. Logan, K. Grossmann, J. Stutz, P. D. Blanken, S. P. Burns, R. Cheng, M. A. Garcia, P. Köhler, S. Lopez, N. C. Parazoo, B. Raczka, D. Schimel, C. Frankenberg, Mechanistic evidence for tracking the seasonality of photosynthesis with solar-induced fluorescence. *Proc. Natl. Acad. Sci. U.S.A.* **116**, 11640–11645 (2019).
46. A. J. Turner, P. Köhler, T. S. Magney, C. Frankenberg, I. Fung, R. C. Cohen, A double peak in the seasonality of California’s photosynthesis as observed from space. *Biogeosciences* **17**, 405–422 (2020).
47. N. Gorelick, M. Hancher, M. Dixon, S. Ilyushchenko, D. Thau, R. Moore, Google Earth Engine: Planetary-scale geospatial analysis for everyone. *Remote Sens. Environ.* **202**, 18–27 (2017).
48. P. J. Crutzen, The role of NO and NO₂ in the chemistry of the troposphere and stratosphere. *Annu. Rev. Earth Planet. Sci.* **7**, 443–472 (1979).
49. A. N. Gruzdev, Latitudinal structure of variations and trends in stratospheric NO₂. *Int. J. Remote Sens.* **30**, 4227–4246 (2009).
50. E. A. Marais, J. F. Roberts, R. G. Ryan, H. Eskes, K. Folkert Boersma, S. Choi, J. Joiner, N. Abuhammad, A. Redondas, M. Grutter, A. Cede, L. Gomez, M. Navarro-Comas, New observations of NO₂ in the upper troposphere from TROPOMI. *Atmos. Meas. Tech.* **14**, 2389–2408 (2021).
51. Y. Zhang, Y. Wang, G. Chen, C. Smeltzer, J. Crawford, J. Olson, J. Szykman, A. J. Weinheimer, D. J. Knapp, D. D. Montzka, A. Wisthaler, T. Mikoviny, A. Fried, G. Diskin, Large vertical gradient of reactive nitrogen oxides in the boundary layer: Modeling analysis of DISCOVER-AQ 2011 observations. *J. Geophys. Res.* **121**, 1922–1934 (2016).
52. J. T. Abatzoglou, S. Z. Dobrowski, S. A. Parks, K. C. Hegewisch, TerraClimate, a high-resolution global dataset of monthly climate and climatic water balance from 1958–2015. *Sci. Data* **5**, 170191 (2018).
53. U. Wood-Sichra, A. B. Joglekar, L. You, “Spatial Production Allocation Model (SPAM) 2005: Technical documentation,” Working paper, HarvestChoice, International Food Policy Research Institute, Washington, D.C., 2016.
54. W. Yuan, Y. Chen, J. Xia, W. Dong, V. Magliulo, E. Moors, J. E. Olesen, H. Zhang, Estimating crop yield using a satellite-based light use efficiency model. *Ecol. Indic.* **60**, 702–709 (2016).

Acknowledgments: We thank the Google Earth Engine team for making large-scale computational resources available to researchers. **Funding:** This work was supported by the NASA Harvest Consortium (NASA Applied Sciences grant no. 80NSSC17K0652, subaward 54308-Z6059203 to D.B.L.) and NSF no. 1715557 and NSF/USDA-NIFA no. 1639318. **Author contributions:** D.B.L. and J.A.B. conceived the study. S.D.T. carried out the analysis with feedback from D.B.L. and J.A.B. D.B.L. drafted the manuscript, and all authors edited the manuscript. **Competing interests:** All authors declare that they have no competing interests. **Data and materials availability:** All data needed to evaluate the conclusions in the paper are present in the paper and/or the Supplementary Materials. Data and replication code for this study are available at <https://doi.org/10.5281/zenodo.6363277>.

Submitted 26 October 2021

Accepted 15 April 2022

Published 1 June 2022

10.1126/sciadv.abm9909